Strength Analysis of a Wing Structure for a Single Turboprop Normal Category Aircraft

Vis Sripawadkul (iD) **and Phacharaporn Bunyawanichakul**

1 Introduction

Developing an aircraft involves a lot of effort regarding the market, technical data, commercial analysis, payload, range, and mission. The aviation sector had been growing rapidly prior to the pandemic in 2019 that has had a major impact not only on aviation but also on the world economy. Now, after almost 2 years, the general aviation sector has started to make a good recovery. The General Aviation Manufacturers Association recently released its aircraft shipment report that indicated a 45.4% increase in turboprop aircraft in the first 6 months of 2021 compared to the same period in 2020, as the highest growth among all types (Table 1).

The objective of this study was to develop a wing geometric model (3D) and perform structural analysis to determine the wing structural requirements and mass for a single turboprop aircraft in the normal category according to 14 Code of Federal Regulations (CFR) Part 23. These requirements are:

- Symmetrical positive and negative limit maneuvering load factor
- Mid-wing stiffness: wing tip displacement <5% of the wing's half span
- Wing mass estimation <12% of maximum take-off weight
- Margin of safety >0.5

In this study, the simplified model of the wing structure was composed of a single box-shaped spar, ribs, and skin with some cutouts excluding stringers and dimensions of control surfaces. The analysis was performed using aluminum as the material, with its structural response for overall strength and tip deformation obtained using finite element analysis.

V. Sripawadkul · P. Bunyawanichakul (✉)
Kasersart University, Bangkok, Thailand
e-mail: fengvisp@ku.ac.th; phacharaporn.b@ku.ac.th

Table 1 First half aircraft shipments and billings

Aircraft type	2020	2021	% change
Piston airplanes	503	565	+12.3%
Turboprops	152	221	+45.4%
Business jets	244	264	+8.2%
Total airplanes	899	1050	+16.8%
Total airplane billing	$7.9B	$8.6B	+9.4%
Piston helicopters	63	83	+31.7%
Turbine helicopters	194	258	+33%
Total helicopters	257	341	+32.7%
Total helicopter billing	$1B	$1.4B	+37.7%

Source: General Aviation Manufacturers Association

1.1 Wing External Geometry

The aircraft had the following specifications:

- Maximum take-off weight   2200 lbs
- Basic empty weight   990 lbs
- Maximum usable fuel   616 lbs
- Maximum usable load   264 lbs
- Engine power   240 hp
- Take-off   1312 ft
- Take-off over 50 ft obstacle   1968 ft
- Climb rate   3000 ft/min
- Maximum operating altitude   28,000 ft
- Stall speed with flaps   61 KCAS
- Maximum cruise speed   320 KTAS
- Landing ground roll   1148 ft
- Wingspan   28.5 ft
- Length   21.0 ft
- Height   8.92 ft
- Cabin width   4.13 ft
- Wing area   95.1 ft^2
- Taper ratio   0.6
- Airfoil   NACA 65_2-415

The wing structural mass was 264 lbs, with the wing incidence angle at root 3 degrees with a −3-degree twist angle.

1.2 Forces on the Wing

1.2.1 Aircraft Flight Envelope (Gust Included)

Referring to Title 14 Code of Federal Regulations (CFR) Part 23, the maximum positive and negative load factors for the normal category are +3.8 and −1.5, respectively. The stall speed was determined at the corresponding maximum lift coefficient of the NACA 65_2-415 airfoil (Airfoil Tools, 2021), while the dive speed was 1.4 times the cruise speed. Gust wind speeds of 50 and 25 fps were included to determine the load factors at cruise speed and dive speed, respectively. The combined flight envelope is shown in Fig. 1.

1.2.2 Critical Forces and Moments

Spanwise lift distribution was calculated using the lifting-line theory initially developed by Prandtl (Sadraey, 2013). First, the wing was divided into N segments along the span with each corresponding angle θ, as shown in Fig. 2.
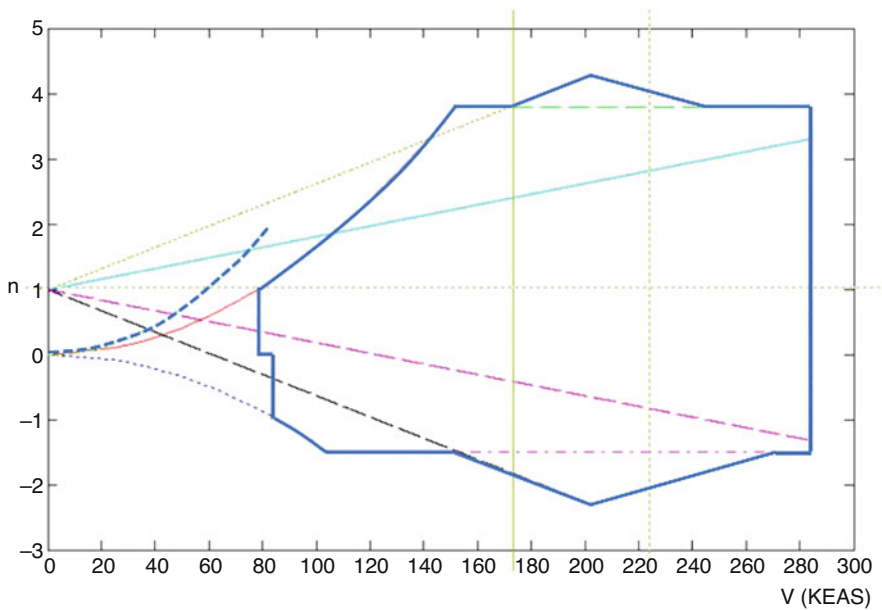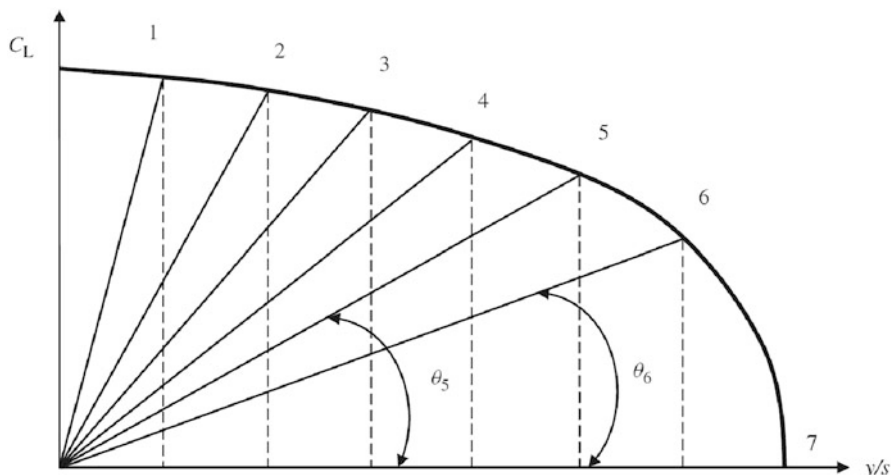

Fig. 1 Combined flight envelope

Fig. 2 Angles corresponding to each segment in lifting-line theory

The aim was to solve for coefficients A_1 to A_n using the following equation:

$$\mu(\alpha - \alpha_0) = \sum_{n=1}^{N} A_n \sin(n\theta)\left(1 + \frac{\mu n}{\sin\theta}\right) \tag{1}$$

where α is the segment's angle of attack and α_0 is the segment's zero-lift angle of attack. The parameter μ is defined as:

$$\mu = \frac{C_i C_{l,\alpha}}{4b} \tag{2}$$

where C_i is the segment's mean geometric chord, $C_{l,\alpha}$ is the segment's lift curve slope, and b is the wingspan. Each segment's lift coefficient was finally determined using the equation:

$$C_{Li} = \frac{4b}{C_i} \sum A_n \sin(n\theta) \tag{3}$$

The shear force and bending moments due to wing structure weight and lift were calculated along spanwise positions at the maximum load factor and with a margin of safety of 0.5 for two flight conditions: cruise and dive. The results of the level flight condition ($n = 1$) are shown in Fig. 3, where the critical shear force and bending moment occur at a dive condition corresponding to 4407 lbs and 312,555 in-lb compared to 2207 lbs and 155,970 in-lb for the dive and maximum cruise speed, respectively. These loads were used as requirements for the wing structure design in the later simulation.
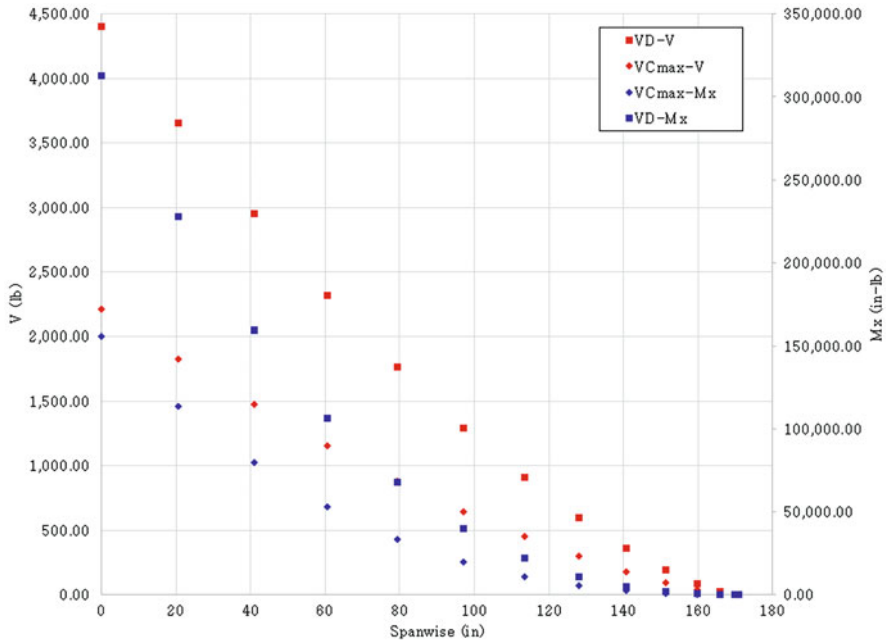
Fig. 3 Wing-bending moment diagram at $n = 1$

## 2 Wing Structure Analysis

2.1 Wing Structural Layout

Only the half wing was modeled due to the symmetry related to the mid-fuselage. The wing model was developed with constant taper and twist and used 7075T6 aluminum sheets, with its material properties shown in Table 2. All wing components in the model were initially developed based on the available thicknesses of the sheet: 0.04″, 0.063″, and 0.125″ (Aircraft Spruce, 2021).

From the wing loading calculation above, all wing components were initially designed and sized using basic theory (Megson, 1999; Brandt et al., 2004) within the framework. Then, several simplified models were developed. For each model, the structural response was simulated and analyzed to fulfill the objectives of this study in terms of strength, deformation, and weight. The wing components were finalized under a skin surface consisting of a single spar and nine ribs (Fig. 4). The spar box running along the wingspan had its center located at 40% of the chord. All ribs were set with uneven spacing according to the non-uniform load distribution with some lightening holes. The model was prepared as a surface with no defined thickness, which was later identified in the pre-processing tool.

Table 2 Properties of 7075T6 aluminum sheet

| Property	Value
Density, lb/in^3	0.101518
Young's modulus, Msi	10
Poisson's ratio	0.33
Yield strength, ksi	64
Ultimate tensile strength, ksi	75
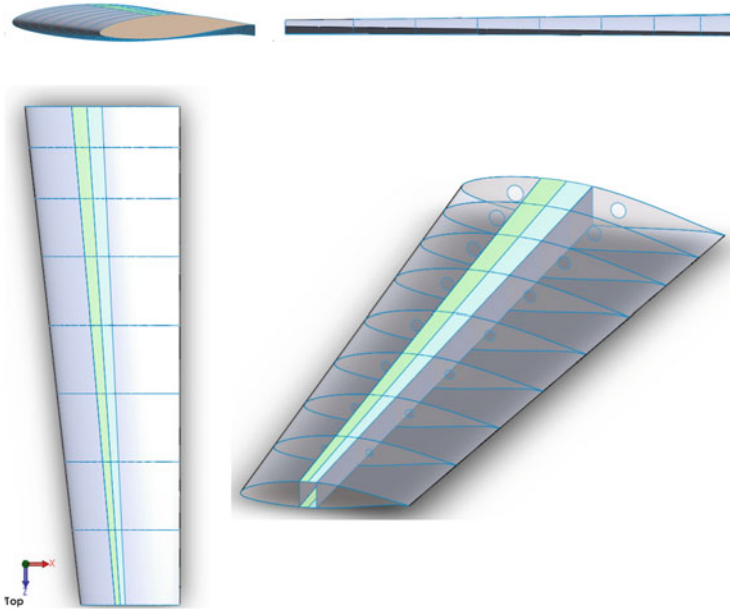
Fig. 4 Wing model from top, side, front, and 3D view

2.2 Thickness Attribution

From the wing simplified model, all wing components were created as 2D shells. The thickness of each part was defined using different colors, as shown in Fig. 5. The identification of the shell type was "thick" when attributing the material to each surface. All skins had a thickness of 0.04″, and the spar webs had a thickness of 0.125″. The thickness of the spar flanges corresponding to bays 1 to 3 from the wing root used three layers of 0.125″ aluminum plate, while the rest of the flanges had only two layers. The four ribs on the root side had a thickness of 0.063″, while the rest had a thickness of 0.04″. The total structural weight was estimated to be 117.97 lbs, which was less than the wing mass estimation (132 lbs).
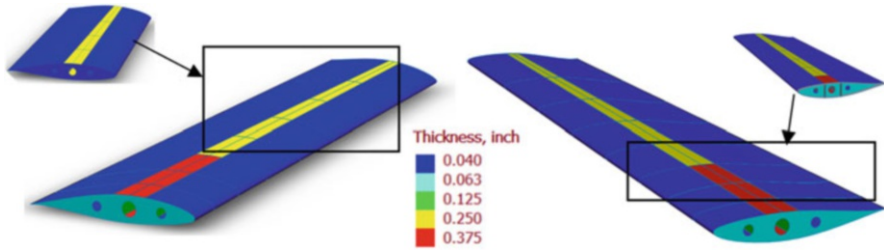
Fig. 5 Thickness of each surface: from top view (left) and bottom isometric view (right)
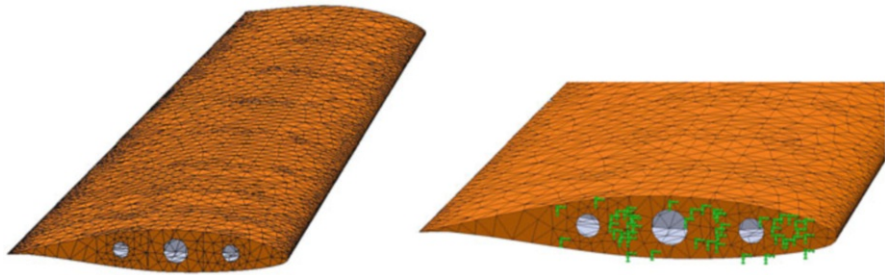
Fig. 6 Wing structure mesh (left) and boundary condition as cantilever beam (right)

2.3 Meshing

All surfaces were divided into several small elements using a curvature-based mesh. The maximum and minimum element sizes were 3″ and 1″, respectively. The general shape of the mesh for the whole wing is shown in Fig. 6. (left) and shows that the outer surface of the model meshing was smooth enough to perform the calculation. The orange color represents the bottom surface of the element, while gray represents the top surface of the element.

2.4 Boundary Conditions

The wing structure was considered as a cantilever boundary condition. The root location was fixed throughout the root rib boundary with no rotation and no displacement to simulate the mounting location to the fuselage as shown by green color in Fig. 6 (right).
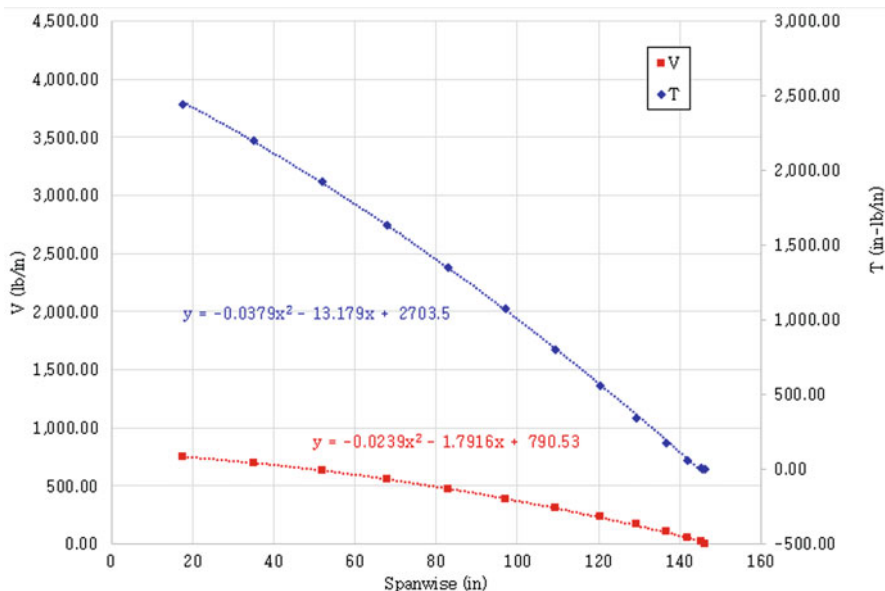
Fig. 7 Shear and torsion along spanwise direction

2.5 Shear Forces and Torsions

The force identified in the previous calculation was applied to the wing model, which was fixed at the root edge as a cantilever beam boundary condition. Figure 7 shows the shear and torsion distribution acting on the wing along a spanwise direction (the z axis as defined in the model).

At a dive speed with the maximum load factor ($n = 3.8$), the total shear force applied on the wing structure was 16,747 lbs. The shear force (V) was varied along the z-direction using the reference coordinates, which were originally located at 40% of the chord length, and was calculated using the equation:

$$V(z) = -2.39 \times 10^{-2}z^2 - 1.792z + 790.53 \tag{4}$$

In the same manner, the pitching moment distribution function was applied to the wing spar about 40% of the chord length with a total intensity of 57,762 in-lb using the equation:

$$T(z) = -3.79 \times 10^{-2}z^2 - 13.18z + 2704 \tag{5}$$

Both the shear and torsion functions were applied to the structure using the non-uniform distribution command. The analysis was performed including gravitational force, as shown in Fig. 8.

Fig. 8 Shear, torsion, and structural body force applied on the structure
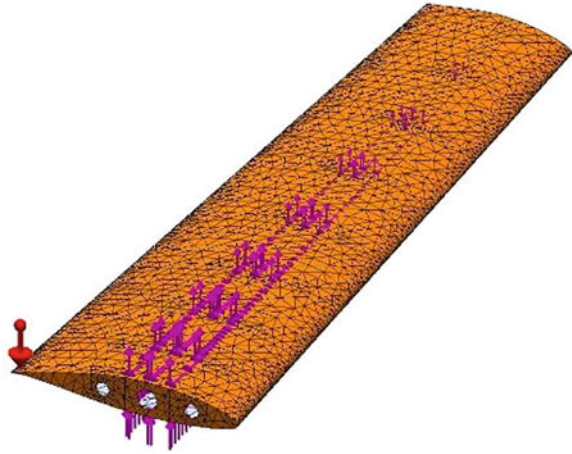
3   Results and Discussion

Static structural analysis was performed, and the outputs in terms of Von Mises stress and displacement are shown in Fig. 9 (left) and Fig. 9 (right), respectively. It was clear that the Von Mises stress was locally high at the wing root because this was the fixed end location from the defined boundary condition. There were some localized stresses at the skin, spar, and rib connection, but the intensity of the stress was not severe. The stress contour showed the region having a margin of safety of 0.5 at the wing-fuselage junction. This region could be reinforced during the manufacturing process.

It was noted that the maximum displacement of 6.48″ occurred at the wing tip which satisfied the constraint of being less than 5% of the wing's half span. The wing gradually twisted and deformed along its spanwise direction.
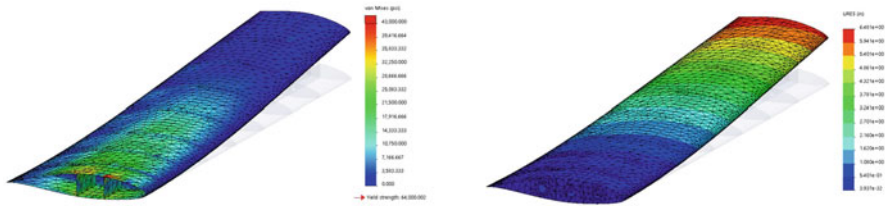
Fig. 9 Von Mises stress of the wing (left) and wing displacement (right)

4   Conclusion and Future Work

Based on the information presented in the flight envelope and the critical wing loading, an initial wing structure was developed that met all aircraft structural and operational requirements according to Title 14 Code of Federal Regulations (CFR) Part 23. The simplified model developed successfully achieved the objectives of this study in terms of strength, displacement, and weight. Further study could include:

- Analysis to include stringers, cutouts, and control surfaces
- Detail design in the high stress concentration region
- Wing design and optimization
- Buckling analysis
- Flutter analysis
- Composite material replacement
- Unsymmetrical flight condition
- Construction and testing of individual components for structural integrity behavior

References

Aircraft Spruce. *General aluminum information*. https://www.aircraftspruce.com/catalog/mepages/aluminfo.php/. Accessed on 10 Mar 2021.

Airfoil 652-415. (2021). *Airfoil tools*. [Online]. Available: http://airfoiltools.com/airfoil/details?airfoil=naca652415-il. Accessed on 1 Mar 2021.

Brandt, S. A., Stiles, R. J., Bertin, J. J., & Withford, R. (2004). *Introduction to aeronautics: A design perspective* (2nd ed.). AIAA Educational Series.

"GAMA", General Aviation Manufacturers Association. https://gama.aero/news-and-events/press-releases/gama-publishes-second-quarter-2021-aircraft-shipments-and-billings-report/. Accessed on 13 Sept 2021.

Megson, T. (1999). *Aircraft structures for engineering students* (3rd ed.). Elsevier.

Sadraey, M. H. (2013). *Aircraft design: A systems engineering approach*. Wiley.